

Measurement of Resonant Frequency and Quality Factor of Microwave Resonators: Comparison of Methods

Paul J. Petersan and Steven M. Anlage

*Center for Superconductivity Research, Department of Physics, University of
Maryland, College Park, MD 20742-4111*

Abstract

Precise microwave measurements of sample conductivity, dielectric, and magnetic properties are routinely performed with cavity perturbation measurements. These methods require the accurate determination of quality factor and resonant frequency of microwave resonators. Seven different methods to determine the resonant frequency and quality factor from complex transmission coefficient data are discussed and compared to find which is most accurate and precise when tested using identical data. We find that the nonlinear least-squares fit to the phase vs. frequency is the most accurate and precise when the signal-to-noise ratio is greater than 65. For noisier data, the nonlinear least squares fit to a Lorentzian curve is more accurate and precise. The results are general and can be applied to the analysis of many kinds of resonant phenomena.

I. INTRODUCTION

Our objective is to accurately and precisely measure the quality factor Q , and resonant frequency f_o , of a microwave resonator, using complex transmission coefficient data as a function of frequency. Accurate Q and f_o measurements are needed for high precision cavity perturbation measurements of surface impedance, dielectric constant, magnetic permeability, etc. Under realistic experimental conditions, corruption of the data occurs because of cross-talk between the transmission lines and between coupling structures, the separation between the coupling ports and measurement device, and noise. Although there are many methods discussed in the literature for measuring Q and resonant frequency, we are aware of no treatment of these different methods which quantitatively compares their accuracy or precision under real measurement conditions. In practice, the Q can vary from 10^7 to 10^3 in superconducting cavity perturbation experiments, so that a Q determination must be robust over many orders of magnitude of Q . Also, it must be possible to accurately determine Q and f_o in the presence of modest amounts of noise. In this paper we will determine the best methods of evaluating complex transmission coefficient data, i.e. the most precise, accurate, robust in Q , and robust in the presence of noise.

Many different methods have been introduced to measure the quality factor and resonant frequency of microwave cavities over the past fifty years. Smith chart methods have been used to determine half power points which can be used in conjunction with the value of the resonant frequency to deduce the quality factor of the cavity.¹⁻⁶ In the decay method for determining the quality factor, the fields in the cavity are allowed to build up to equilibrium, the input power is turned off, and the exponential decrease in the power leaving the cavity is measured and fit to determine the quality factor of the cavity.^{3,4,7,8}

Cavity stabilization methods put the cavity in a feedback loop to stabilize an oscillator at the resonant frequency of the cavity.⁸⁻¹² For one port cavities, reflection measurements provide a determination of the half power points and also determine the coupling constant, allowing one to calculate the unloaded Q .¹³⁻¹⁶ In more recent years, complex transmission

coefficient data vs. frequency is found from vector measurements of transmitted signals through the cavity.^{17–20} Methods which use this type of data to determine Q and f_o are the subject of this paper.

We have selected seven different methods for determining f_o and Q from complex transmission coefficient data. We have collected sets of 'typical' data from realistic measurement situations to test all of the Q and f_o determination methods. We have also created data and added noise to it to measure the accuracy of the methods. In this paper we consider only random errors and not systematic errors, such as vibrations of the cavity which artificially broaden the resonance.^{8–12} After comparing all of the different methods, we find that the nonlinear least squares fit to the phase vs. frequency and the nonlinear least squares fit of the magnitude of the transmission coefficient to the Lorentzian curve are the best methods for determining the resonant frequency and quality factor. The phase vs. frequency fit is the most precise and accurate over many decades of Q values if the signal-to-noise ratio (SNR) is high (SNR > 65), however the Lorentzian fit is more robust for noisier data. Some of the methods discussed here rely on a circle fit to the complex transmission coefficient data as a step to finding f_o and Q . We find that by adjusting this fitting we can improve the determination of the quality factor and resonant frequency, particularly for noisy data.

In section II of this paper, the simple lumped element model for a microwave resonator is reviewed and developed. A description of our particular experimental setup is then given, although the results of this paper apply to any transmission resonator. We then discuss the data collected and generated for use in the method comparison in section III. Section IV outlines all of the methods that are studied in this paper. It should be noted that each method is tested using exactly the same data. The results of the comparison are presented and discussed in section V. Possible improvements for some of the methods follow in section VI, and the concluding remarks of the paper are made in the final section.

II. LUMPED ELEMENT MODEL OF A RESONATOR

To set the stage for our discussion of the different methods of determining

Q and resonant frequency, we briefly review the simple lumped-element model of an electromagnetic resonator. As a model for an ideal resonator, we use the series RLC circuit (see inset of Fig. 1), defining $1/2\pi\sqrt{LC}$ as the resonant frequency f_o .¹⁹ The quality factor is defined as 2π times the ratio of the total energy stored in the resonator to the energy dissipated per cycle.⁴ For the lumped element model in Fig. 1, the quality factor Q is $2\pi f_o L/R$. The resonator is coupled to transmission lines of impedance Z_o by the mutual inductances l_{m1} and l_{m2} . The complex transmission coefficient, S_{21} (ratio of the voltage transmitted to the incident voltage), as a function of driving frequency f , is given in the limit of weak coupling by:¹⁹

$$S_{21}(f) = \frac{\overline{S_{21}}}{1 + iQ \left(\frac{f}{f_o} - \frac{f_o}{f} \right)} \quad (1)$$

The additional assumption that $f \sim f_o$ near resonance simplifies the frequency dependence in the denominator resulting in:

$$S_{21}(f) = \frac{\overline{S_{21}}}{1 + i2Q \left(\frac{f}{f_o} - 1 \right)} \quad (2)$$

where $\overline{S_{21}}$ is the maximum of the transmission coefficient which occurs at the peak of the resonance:

$$\overline{S_{21}} = \frac{8\pi^2 f^2 l_{m1} l_{m2}}{Z_o R} = 2\sqrt{\beta_1 \beta_2} \quad (3)$$

Here R is the resistance in the circuit model and this expression again is valid in the weak coupling limit. On the far right side of Eq. (3), β_1 and β_2 are the coupling coefficients on ports 1 and 2, respectively,^{3,20} where $\beta_j = (2\pi f)^2 l_{mj}^2 / Z_o R$, with $j = 1, 2$. The magnitude of the complex transmission coefficient is:

$$|S_{21}(f)| = \frac{|\overline{S_{21}}|}{\sqrt{1 + 4Q^2 \left(\frac{f}{f_o} - 1 \right)^2}} \quad (4)$$

The plot of $|S_{21}|$ vs. frequency forms a Lorentzian curve with the resonant frequency located at the position of the maximum magnitude (Fig. 1). A numerical investigation of $|S_{21}|$ with and without the simplified denominator assumption leading to Eq. (2), shows that even for a relatively low Q ($Q = 100$), the difference between the magnitudes is less than half a percent of the magnitude using Eq. (1). For larger Q the difference is much smaller, so we take this assumption as valid. All of the analysis methods treated in this paper make use of the simplified denominator assumption, as well as all the data we create to test the methods.

The plot of the imaginary part of S_{21} (Eq. (2)) versus the real part (with frequency as a parameter), forms a circle in canonical position with its center on the real axis (Fig. 2). The circle intersects the real axis at two points, at the origin and at the location of the resonant frequency.

Important alterations to the data occur when we take into account several aspects of the real measurement situation. The first modification arises when considering the cross talk between the cables and/or the coupling structures. This introduces a complex translation $X = (x_o, y_o)$, of the center of the circle away from its place on the real axis.^{19,20,21} Secondly, a phase shift ϕ is introduced because the coupling ports of the resonator do not necessarily coincide with the plane of the measurement. This effect rotates the circle around the origin (Fig. 2).^{19,20,21} The corrected complex transmission coefficient, \tilde{S}_{21} , is then given by:

$$\tilde{S}_{21} = (S_{21} + X) e^{i\phi} \quad (5)$$

It should be noted that the order in which the translation and rotation are performed is unique.²¹

Any method of determining Q and f_o from complex transmission data must effectively deal with the corruption of the data represented by Eq. (5). In addition, the method used to determine f_o and Q must give accurate and precise results even in the presence of noise. This is necessary since, in typical measurements, Q ranges over several orders of magnitude causing the signal-to-noise ratio (SNR, defined in section III. c.) during a single data run to

vary significantly. Further corruption of the data can occur if there are nearby resonances present, particularly those with lower Q . This introduces a background variation onto the circles shown in Fig. 2 and may interfere with the determination of f_o and Q . In this paper we consider only single isolated resonances and refer the reader to an existing treatment of multiple resonances.²⁷

III. DATA USED FOR METHOD COMPARISON

In this section we discuss the data we use for making quantitative comparisons of each method. The data is selected to be representative of that encountered in real measurement situations. Each trace consists of 801 frequency points, each of which have an associated real and imaginary part of S_{21} . Two types of data have been used for comparing the methods; measured data and generated data. The measured data is collected with the network analyzer and cavity described below. The generated data is constructed to look like the measured data, but the underlying Q and resonant frequency are known exactly. All of the methods discussed in the next section are tested using exactly the same data.

A. Measured Data

Complex transmission coefficient vs. frequency data is collected using a superconducting cylindrical Niobium cavity submerged in liquid Helium at 4.2 K. Microwave coupling to the cavity is achieved using magnetic loops located at the end of 0.086" coaxial cables. The loops are introduced into the cavity with controllable position and orientation. The coaxial cables come out of the cryogenic dewar and are then connected to an HP8510C vector network analyzer.²² The cavity design²³ has recently been modified to allow top-loading of the samples into the cavity.

A sample is introduced into the center of the cavity on the end of a sapphire rod. The temperature of the sample can be varied by heating the rod, with a minimal perturbation to the superconducting Nb walls. The quality factor of the cavity

resonator in the TE_{011} mode can range from about 2×10^7 to 1×10^3 , with a resonant frequency of approximately 9.6 GHz. In a typical run with a superconducting crystal, where the temperature varies from 4.2 K to 200 K, f_o decreases by about 10 MHz and Q changes from about 1×10^7 to 4×10^3 . For accurate measurement of the electrodynamic properties of samples, it is important to be able to resolve frequency shifts of the cavity as small as 1 Hz at low temperatures.

1. Fixed Powers

One hundred S_{21} vs. frequency traces were taken using the network analyzer held at a fixed power and with constant coupling to the cavity. One such data set was made with the source power at +15 dBm (SNR \approx 368, $f_o \approx$ 9.600242 GHz, $Q \approx 6.39 \times 10^6$), another set was taken with the source power at +10 dBm (SNR \approx 108, $f_o \approx$ 9.599754 GHz, $Q \approx 6.46 \times 10^6$), a third data set was taken with the source power at +3 dBm (SNR \approx 49, $f_o \approx$ 9.599754 GHz, $Q \approx 6.50 \times 10^6$). (The approximate values for f_o and Q are obtained from the phase vs. frequency averages discussed below)

2. Power Ramp

To collect data with a systematic variation of signal-to-noise ratio, we took single traces at a series of different input powers. A power-ramped data set was taken in a cavity where controllable parameters, such as temperature and coupling, were fixed, the only thing that changed was the microwave power input to the cavity. An S_{21} vs. frequency trace was taken for powers ranging from -18 dBm to $+15$ dBm, in steps of 0.5 dBm. This corresponds to a change in the signal-to-noise ratio from about 5 to 168 ($f_o \approx$ 9.603938 GHz, $Q \approx 8.71 \times 10^6$).

B. Generated Data

To check the accuracy of all the methods, we generated data with known characteristics, and added a controlled amount of noise to simulate the measured data. The data was created using the real and imaginary parts of an ideal S_{21} as a function of frequency Eq. (2);

$$\operatorname{Re} S_{21}(f) = \frac{\overline{S_{21}}}{1 + 4Q^2 \left(\frac{f}{f_o} - 1\right)^2} \quad \operatorname{Im} S_{21}(f) = \frac{-\overline{S_{21}}2Q \left(\frac{f}{f_o} - 1\right)}{1 + 4Q^2 \left(\frac{f}{f_o} - 1\right)^2} \quad (6)$$

Where $\overline{S_{21}}$ is the diameter of the circle being generated (see Fig. 2), Q is the quality factor, and f_o is the resonant frequency, which are all fixed. The frequency f , is incremented around the resonant frequency to create the circle. There are 400 equally spaced frequency points before and after the resonant frequency, totaling 801 data points. The total span of the generated data is about four 3dB bandwidths for all Q values.

To simulate measured data, noise was added to the data using Gaussian distributed random numbers²⁴ that were scaled to be a fixed fraction of the radius, r of the circle described by the data in the complex S_{21} plane. The noisy data was then translated and rotated to mimic the effect of cross talk in the cables and coupling structures, and delay (Eq. (5)).

1. Power Ramp

A power ramp was simulated by varying the amplitude of the noise added to the circles. A total of 78 S_{21} vs. frequency traces were created with a variation of the signal-to-noise ratio from about 1 to 2000 ($f_o = 9.600$ GHz, $Q = 1.00 \times 10^6$, $x_o = 0.1972$, $y_o = -0.0877$, $r = 0.2$, $\phi = \pi/17$)

2. Fixed Q Values

Data with different fixed Q values were created using the above real and imaginary expressions for S_{21} . Groups of data were created with 100 traces each using: $Q = 10^2, 10^3$,

10^4 , 10^5 ($f_o = 9.600$ GHz and $\text{SNR} \approx 65$ for all sets). They include fixed noise amplitude, and were each rotated and translated equal amounts to simulate measured data. ($x_o = 0.01$, $y_o = 0.015$, $r = 0.2$, $\phi = \pi/19$)

C. Signal-to-Noise Ratio

The signal-to-noise ratio was found for all data sets by first determining the radius r_{circle} , and center (x_c, y_c) of the circle when plotting the imaginary part of the complex transmission coefficient vs. the real part (Fig. 2). Next, the distance to each data point (x_i, y_i) ($i = 1$ to 801) from the center is calculated from:

$$d_i = \sqrt{(x_i - x_c)^2 + (y_i - y_c)^2} \quad (7)$$

The signal-to-noise ratio is defined as:

$$\text{SNR} = \frac{r_{circle}}{\sqrt{\frac{1}{800} \sum_{i=1}^{801} (d_i - r_{circle})^2}} \quad (8)$$

In the case of generated data, where the center and radius of the circle are known, the SNR is very well defined. However, the SNR values are approximate for the measured data because of uncertainties in the determination of the center and radius of the circles.

IV. DESCRIPTION OF METHODS

In this section we summarize the basic principles of the leading methods for determining the Q and resonant frequency from complex transmission coefficient vs. frequency data. Further details on implementing these particular methods can be found in the cited references. Because we believe that this is the first published description of the inverse mapping technique, we shall discuss it in more detail than the other methods. The Resonance Curve Area and Snortland techniques are not widely known, hence a brief review of these methods is also included.

The first three methods take the data as it appears and determine the Q from the estimated bandwidth of the resonance. The last four methods make an attempt to first correct the data for rotation and translation (Eq. (5)), then determine f_o and Q of the data in canonical position.

A. 3 dB Method

The 3 dB method uses the $|S_{21}|$ vs. frequency data (Fig. 1), where $|S_{21}| = \sqrt{(\text{Re } S_{21})^2 + (\text{Im } S_{21})^2}$. The frequency at maximum magnitude is used as the resonant frequency, f_o . The half power points ($\frac{1}{\sqrt{2}} \max |S_{21}|$) are determined on either side of the resonant frequency and the difference of those frequency positions is the bandwidth Δf_{3dB} . The quality factor is then given by:

$$Q = f_o / \Delta f_{3dB} \quad (9)$$

Because this method relies solely on the discrete data, not a fit, it tends to give poor results as the signal-to-noise ratio decreases.

B. Lorentzian Fit

For this method, the $|S_{21}|$ vs. frequency data is fit to a Lorentzian curve (Eq. (4) and Fig. 1) using a nonlinear least squares fit.²⁵ The resonant frequency f_o , bandwidth Δf_{Lorent} , constant background A_1 , slope on the background A_2 , skew A_3 , and maximum magnitude $|S_{\max}|$ are used as fitting parameters for the Lorentzian:

$$|S_{21}(f)| = A_1 + A_2 f + \frac{|S_{\max}| + A_3 f}{\sqrt{1 + 4 \left(\frac{f - f_o}{\Delta f_{Lorent}} \right)^2}} \quad (10)$$

The least squares fit is iterated until the change in chi squared is less than 1 part in 10^3 . The Q is then calculated using the values of f_o and Δf_{Lorent} from the final fit parameters: $Q = f_o / \Delta f_{Lorent}$. This method is substantially more robust in the presence of noise than

the 3 dB method. For purposes of comparison with other methods, we shall use the simple expressions for f_o and Q given above, rather than the values modified by the skew parameter.

C. Resonance Curve Area Method

In an attempt to use all of the data, but to minimize the effects of noise in the determination of Q , the Resonance Curve Area (RCA) method was developed.²⁶ In this approach the area under the $|S_{21}(f)|^2$ curve is integrated to arrive at a determination of Q . In detail, the RCA method uses the magnitude data squared, $|S_{21}|^2$, versus frequency and fits it to a Lorentzian peak (same form as Fig. 1):

$$|S_{21}(f)|^2 = \frac{P_o}{1 + 4 \left(\frac{f-f_o}{\Delta f_{RCA}} \right)^2} \quad (11)$$

using the resonant frequency, f_o , and the maximum magnitude squared, P_o , as fitting parameters. The bandwidth Δf_{RCA} is a parameter in the Lorentzian fit, but is not allowed to vary. This method iterates the Lorentzian fit until chi squared changes by less than 1 part in 10^4 . Next, using the fit values from the Lorentzian, the squared magnitude $|S_{21}(f_o \pm f_r)|^2$ is found at two points $f_o \pm f_r$ on the tails of the Lorentzian far from the resonant frequency. The area under the data, S_1 , from $f_o - f_r$ to $f_o + f_r$ (symmetric positions on either side of the resonant frequency) is found using the trapezoidal rule:²⁴

$$S_1 = \int_{f_o-f_r}^{f_o+f_r} |S_{21,data}(f)|^2 df = \sum_{N=f_o-f_r}^{f_o+f_r} \frac{\delta f}{2} \left(|S_{21,data}(N)|^2 + |S_{21,data}(N+1)|^2 \right) \quad (12)$$

Here $|S_{21,data}(N)|^2$ indicates the magnitude squared data point at the frequency N , and δf is the frequency step between consecutive data points.

The quality factor is subsequently computed from the area as follows:²⁶

$$Q = f_o \frac{P_o}{S_1} \tan^{-1} \sqrt{\frac{P_o}{|S_{21}(f_o \pm f_r)|^2} - 1} \quad (13)$$

This Q is compared to the previously determined one. If Q changes by more than 1 part in 10^4 , the Lorentzian fit is repeated using as initial guesses for f_o and P_o , the values of

f_o and P_o from the previous Lorentzian fit, but the fixed value of the bandwidth becomes $\Delta f_{RCA} = f_o/Q$. With the new returned parameters from the fit, Q is again computed by Eqs. (12) and (13) and compared to the previous one, and the cycle continues until convergence on Q is achieved. This method is claimed to be more robust against noise because it uses all of the data in the integral given in Eq. (12).²⁶

All of the above methods assume a simple Lorentzian-like appearance of the $|S_{21}|$ vs. frequency data. However, the translation and rotation of the data described by Eq. (5) can significantly alter the appearance of $|S_{21}|$ vs. frequency. In addition, other nearby resonant modes can dramatically alter the appearance of $|S_{21}|$.²⁷ For these reasons, it is necessary, in general, to correct the measured S_{21} data to remove the effects of cross-talk, delay, and nearby resonant modes. The remaining methods in the section all address these issues before attempting to calculate the Q and resonant frequency.

D. Inverse Mapping Technique

1. Circle Fit

The inverse mapping technique, as well as all subsequent methods in this section, make use of the complex S_{21} data and fit a circle to the plot of $\text{Im}(S_{21})$ vs. $\text{Re}(S_{21})$ (Fig. 2). The details of fits of complex S_{21} data to a circle have been discussed before by several authors.^{17,19} The data is fit to a circle using a linearized least-squares algorithm. In the circle fit, the data is weighted by first locating the point midway between the first and last data point; this is the reference point (x_{ref}, y_{ref}) (see Fig. 2). Next, the distance from the reference point to each data point (x_i, y_i) is calculated. A weight is then assigned to each data point ($i = 1$ to 801) as:

$$W_{Map,i} = \left[(x_{ref} - x_i)^2 + (y_{ref} - y_i)^2 \right]^2 \quad (14)$$

This gives the points closer to the resonant frequency a heavier weight than those further away. The circle fit determines the center and radius of a circle which is a best fit to the

data.

2. Inverse Mapping

We now know the center and radius of the circle which has suffered translation and rotation, as described by Eq. (5). Rather than un-rotating and translating the circle back into canonical position, this method uses the angular progression of the measured points around the circle (as seen from the center) as a function of frequency to extract the Q and resonant frequency.²⁸ Three data points are selected from the circle, one randomly chosen near the resonant frequency (f_2), and two others (f_1 and f_3) randomly selected but approximately 1 bandwidth above and below the resonant frequency (see Fig. 3 (b)). Figure 3 (a) shows the complex frequency plane with the measurement frequency axis ($\text{Im } f$) and the pole of interest at a position $if_o - \Delta f_{Map}/2$. The conformal mapping defined by:

$$S_{21} = \frac{\overline{S_{21}} \Delta f_{Map}/2}{f - \left(if_o - \frac{\Delta f_{Map}}{2} \right)} \quad (15)$$

maps the imaginary frequency axis into a circle in canonical position in the S_{21} plane (this mapping is obtained from Eq. (2) by rotating the frequency plane by $e^{-i\pi/2}$). Under this transformation, a line passing through the pole in the complex frequency plane (such as the line connecting the pole and if_2 in Fig. 2 (a)) will map into a line of equal but opposite slope through the origin in the S_{21} plane.²⁹ In addition, because the magnitudes of the slopes are preserved, the angles between points f_1 and f_2 (θ_1), and points f_2 and f_3 (θ_2), in the S_{21} plane (Fig. 3 (b)) are exactly the same as those subtended from the pole in the complex frequency plane (Fig. 3 (a)).³⁰ The angles subtended by these three points, as seen from the center of the circle in the S_{21} plane, define circles in the complex frequency plane which represent the possible locations of the resonance pole (dashed circles in Fig. 3 (a)).^{28,31} The intersection of these two circles off of the imaginary frequency axis uniquely locates the resonance pole. The resonant frequency and Q are directly calculated from the pole position in the complex frequency plane as f_o and $f_o/\Delta f_{Map}$. This procedure is repeated many times

by again choosing three data points as described above, and the results for Q and resonant frequency are averaged.

E. Modified Inverse Mapping Technique

We find that the fit of the complex S_{21} data to a circle is critically important for the quality of all subsequent determinations of Q and f_o . Hence we experimented with different ways of weighting the data to accomplish the circle fit. The modified inverse mapping technique is identical to the previous inverse mapping, except for a difference in the weighting schemes for the fit of the data to a circle (Fig. 2). Here the weighting on each data point, known as the standard weighting, is:

$$W_{Std,i} = \left[(x_{ref} - x_i)^2 + (y_{ref} - y_i)^2 \right] \quad (16)$$

and is the square root of the weighting in Eq. (14). Other kinds of weighting will be discussed in section VI.

F. Phase versus Frequency Fit

In the phase vs. frequency fit,¹⁹ the complex transmission data is first fit to a circle as discussed above for the inverse mapping technique. In addition, an estimate is made of the rotation angle of the circle. The circle is then rotated and translated so that its center lies at the origin of the S_{21} plane (rather than canonical position), and an estimation of the resonant frequency is found from the intersection of the circle with the positive real axis (see Fig. 4 inset). The phase angle of every data point with respect to the positive real axis is then calculated. Next the phase as a function of frequency (Fig. 4), obtained from the ratio of the two parts of Eq. (6), is fit to this form using a nonlinear least-squares fit:²⁴

$$\phi(f) = \phi_o + 2 \tan^{-1} \left[2Q \left(1 - \frac{f}{f_o} \right) \right] \quad (17)$$

In this equation ϕ_o , the angle at which the resonant frequency occurs, f_o , and Q are determined from the fit.³² A weighting is used in the fit to emphasize data near the resonant frequency and discount the noisier data far from the resonance which shows little phase variation. Again we find that the quality of this fit is sensitive to the method of fitting the original S_{21} data to a circle.

G. Snortland Method

As will be shown below, the main weakness of the Inverse Mapping and Phase versus Frequency methods is in the initial circle fit of the complex S_{21} data. To analyze the frequency dependence of the data, or to bring the circle back into canonical position for further analysis, the center and rotation angle (Eq. 5) must be known to very high precision. The Snortland method makes use of internal self-consistency checks on the data to make fine adjustments to the center and rotation angle parameters, thus improving the accuracy of any subsequent determination of the resonant frequency and Q .

The Snortland method²¹ starts with a standard circle fit and phase vs. frequency fit (Fig. 4) as discussed above. A self-consistency check is made on the S_{21} data vs. frequency by making use of the variation of the stored energy in the resonator as the frequency is scanned through resonance. As the resonant frequency is approached from below, the current densities in the resonator increase. Beyond the resonant frequency they decrease again. Hence a sweep through the resonance is equivalent to an increase and decrease of stored energy in the cavity and power dissipated in the sample. In general, there is a slight nonlinear dependence of the sample resistance and inductance on resonator current I . This leads to a resonant frequency and quality factor which are current-level dependent. The generalized expression for a resonator with current-dependent resonant frequency and Q is²¹

$$s \equiv \frac{S_{21}(\omega, I)}{S_{21}(\omega_{\max}, I_{\max})} = \frac{1}{\frac{Q_{\max}}{Q(I)} + i2Q_{\max} \left(\frac{\omega - \omega_o(I)}{\omega_o(I)} \right)} \quad (18)$$

where ω_{\max} and Q_{\max} are the resonant frequency and Q at the point of maximum current

in the resonator, I_{\max} . The Q and resonant frequency are therefore determined at every frequency point on the resonance curve as²¹

$$Q(I) = \frac{Q_{\max}}{\text{Re}[s^{-1}]} \quad (19)$$

$$\omega_o(I) = \frac{\omega}{[1 + \text{Im}[s^{-1}]/2Q_{\max}]} \quad (20)$$

If it is assumed that the response of the resonator is non-hysteretic as a function of power, then the up and down "power ramps" must give consistent values for the Q and resonant frequency at each current level. If the data is corrupted by a rotation in the S_{21} plane, the slight nonlinear response of Q and f_o with respect to field strength causes the plots of Q and f_o vs. the current level to trace out hysteresis curves.²¹ By adjusting the rotation phase angle and Q_{\max} parameters, one can make the two legs of the $Q(I)$ and $\omega_o(I)$ curves coincide, thereby determining the resonant frequency and Q more precisely.²¹

In practice, the resonant frequency is determined from a fit to the non-linear inductance as a function of resonator current I through $\omega(I)^{-2} = c_0 + c_1 I$ so that $\omega_{\max} = 1/\sqrt{c_0 + c_1 I_{\max}}$. Q_{\max} is determined by making the two legs of the $\omega_o(I)$ curve overlap. The resulting determination of resonant frequency and quality factor are ω_{\max} and Q_{\max} , respectively.

V. COMPARING METHODS AND DISCUSSION

The values of Q and f_o obtained by each method for a group of data (e.g. fixed power or fixed Q) are averaged and their standard deviations are determined. These results are used to compare the methods. The accuracy of each method is determined using the generated data since, in those cases, the true values for Q and f_o are known. The most accurate method is simply the one that yields an average $(\overline{f_o}, \overline{Q})$ closest to the actual value $(f_o^{\text{known}}, Q^{\text{known}})$. The standard deviations (σ_{f_o}, σ_Q) for the measured data are used as a measure of precision for the methods. The smaller the standard deviation returned, the more precise the method. To determine the most robust method over a wide dynamic range of Q and

noise, both accuracy and precision are considered. Hence the algorithm that is both accurate and precise over varying Q or noise is deemed the most robust.

A. Fixed Power Data

Figures 5 and 6 show the values of f_o and Q respectively, resulting from the Lorentzian fit (B), the modified inverse mapping technique (E), and the phase vs. frequency fit (F), for the +10 dBm (SNR ≈ 108) fixed power run. For f_o , all three methods return values that are very close to each other. This is verified by the ratios of $\sigma_{f_o}/\overline{f_o}$ for those methods shown in Table I, which shows the normalized ratio (normalized to the lowest number) of the standard deviation of f_o and Q to their average ($\sigma_{f_o}/\overline{f_o}$, σ_Q/\overline{Q}) returned by each method on identical data. The difference in f_o from trace to trace, seen in Fig. 5 is due entirely to the particular noise distribution on that $S_{21}(f)$ trace. On the other hand, the determinations of Q are very different for the three methods. From Fig. 6, we see that the phase vs. frequency fit is more precise in finding Q than both the Lorentzian fit and the modified inverse mapping technique (see also Table I). Thus the fixed power data identifies the phase vs. frequency fit as the best.

B. Power-Ramped Data

Figures 7 and 8 show the results for f_o and Q respectively, from the same methods, for the measured power-ramped data sets. The data are plotted vs. the signal-to-noise ratio (SNR) discussed in section III. As the SNR decreases, the determination of f_o becomes less precise, but as in the case of fixed power, all of the methods return similar ratios for $\sigma_{f_o}/\overline{f_o}$ as confirmed by Table I. The determination of Q also becomes less precise as the SNR decreases tending to overestimate its value for noisier data. But, from Fig. 8, we see that while the modified inverse mapping technique and phase vs. frequency fit give systematically increasing values of Q as the SNR decreases, the Lorentzian fit simply jumps around the average value. This implies that for a low SNR, the Lorentzian fit is a more precise method.

Table I confirms this statement by showing that the Lorentzian fit has the smallest ratio of σ_Q/\overline{Q} . We thus conclude that over a wide dynamic range of SNR the Lorentzian fit is superior, although the phase vs. frequency fit is not significantly worse.

From figures 7 and 8, we see that the f_o determination does not degrade nearly as much as the Q determination as SNR decreases. Here, $\sigma_{f_o}/\overline{f_o}$ changes by a factor of 2, while σ_Q/\overline{Q} changes by a factor of 300 as SNR decreases from 100 to 3, so the precision in the determination f_o is much greater than that of Q . The trend of decreasing Q as the SNR increases beyond a value of about 50 in Fig. 8 is most likely due to the non-linear resistance of the superconducting walls in the cavity. An analysis of generated data power-ramps does not show a decreasing Q at high SNR.

C. Precision, Accuracy, and Robustness

The most precise methods over different fixed powers are the nonlinear least squares fit to the phase vs. frequency (F) and the Lorentzian nonlinear least squares fit (B) (Table I). They consistently give the smallest ratios of their standard deviation to their average for both Q and f_o compared to all other methods. At high power (SNR > 350) the phase vs. frequency fit is precise to about 3 parts in 10^{10} for the resonant frequency and to 3 parts in 10^4 for the quality factor, when averaged over about 75 traces.

When looking at the generated data with SNR ≈ 65 , the most accurate method for the determination of the resonant frequency is the phase vs. frequency fit, because it returns an average closest to the true value, or as in Table II, it has the smallest ratio of the difference between the average and the known value divided by the known value ($\frac{|\overline{f_o} - f_o^{known}|}{f_o^{known}}$, $\frac{|\overline{Q} - Q^{known}|}{Q^{known}}$). The value returned for the resonant frequency is accurate to about 8 parts in 10^8 for $Q = 10^3$, and 1 part in 10^9 for $Q = 10^5$ when averaged over 100 traces. For the quality factor, the phase vs. frequency fit (F) is most accurate (Table II), with accuracy to about 1 part in 10^4 for $Q = 10^3$, and 1 part in 10^4 for $Q = 10^5$ when averaged over 100 traces.

The method most robust in noise is the Lorentzian fit (see the power ramp columns of both Tables). It provided values for f_o and Q that were the most precise and accurate as the signal-to-noise ratio decreased (particularly for $\text{SNR} < 10$). Over several decades of Q , the most robust method for the determination of f_o is the phase vs. frequency fit, which is precise to about 1 part in 10^5 when $Q = 10^2$, and to about 1 part in 10^8 when $Q = 10^5$, averaged over 100 traces with $\text{SNR} \approx 65$. For the determination of Q , the phase vs. frequency (F) is also the most robust, providing precision to 2 parts in 10^3 when $Q = 10^2$ to 10^5 averaged over 100 traces.

VI. IMPROVEMENTS

The first three methods discussed above (3dB, Lorentzian fit, and RCA method) can be improved by correcting the data for rotation and translation in the complex S_{21} plane. All of the remaining methods can be improved by carefully examining the validity of the circle fit. We have observed that by modifying the weighting we can improve the fit to the circle for noisy data, and thereby improve the determination of Q and f_o . For instance, Fig. 9 shows that the standard weighting (the weighting from the modified inverse mapping technique) systematically overestimates the radius of the circle for noisy data. Below we discuss several ways to improve these fits.

By introducing a radial weighting, we can improve the circle fit substantially (an example is shown in Fig. 9). For the radial weighting, we first do the standard weighting to extract an estimate for the center of the circle (x_c, y_c) , which is not strongly corrupted by noise. The radial weighting on each point ($i = 1$ to 801) is then defined as:

$$W_{Radial,i} = \frac{1}{\sqrt{(x_c - x_i)^2 + (y_c - y_i)^2}} \quad (21)$$

which reduces the influence of noisy data points well outside the circle. Figure 10 shows a plot of the calculated radius versus the signal-to-noise ratio for the generated power-ramped data set. The figure shows plots of the calculated radius using four different weightings:

W_{std} (Eq. (16)), W_{Radial} (Eq. (21)), $W_{Radial}^{1/2}$, and W_{Radial}^2 . From this plot, it is clear that above a SNR of about 30 all of the weightings give very similar radius values. However, below that value we see that the radius from the $W_{Radial}^{1/2}$ weighting agrees best with the true radius of 0.2. Therefore, by improving the circle fit with a similar weighting scheme, we hope to extract even higher precision and better accuracy from these methods at lower signal-to-noise ratio.

In addition to errors in the fit radius of the circle at low SNR, there can also be errors in the fit center of the circle. Figure 11 shows the normalized error, E_c :

$$E_c = \sqrt{\left(\frac{x_c - x_{fit}}{x_c}\right)^2 + \left(\frac{y_c - y_{fit}}{y_c}\right)^2} \quad (22)$$

in the calculation of the center of the circle from weightings: W_{std} , W_{Radial} , $W_{Radial}^{1/2}$, and W_{Radial}^2 , vs. the SNR in log scaling. Here (x_c, y_c) is the true center of the circle and (x_{fit}, y_{fit}) is the calculated center from the circle fit. From Fig. 11, we see that the calculation of the center of the circle is accurate to within 1% for SNR ≈ 20 and above using any weighting. However, below SNR = 10, all of the weightings give degraded fits. The inset (b) of Fig. 11 shows the angle α vs. SNR, where α is the angle between the vector connecting the true and calculated centers, and the vector connecting the true center to the position of the resonant frequency. From this figure we see that the angle between these vectors approaches π as SNR decreases, which means that the fit center migrates in the direction away from the resonant frequency as the data becomes noisy. This indicates that the points on the side of the circle opposite from the resonant frequency have a combined weight larger than those points around the resonant frequency, and thus the center is calculated closer to those points.

For data with SNR greater than about 10, all weightings give similar results for the circle fits. For data with SNR less than 10, the best circle fit would make an estimate of the radius of the circle by using the square root radial weighting, and an estimate of the center by weighting data near the resonant frequency more heavily.

A further refinement of the inverse mapping method would be to fit the data with an

arbitrary number of poles and zeroes to take account of multiple resonances in the frequency spectrum.³¹

The Snortland method was originally developed to analyze non-linear resonances.²¹ Our use of it for linear low-power resonances was preliminary, and the results probably do not reflect its ultimate performance. Further development of this method on linear resonances has the potential to produce results superior to those obtained with the phase vs. frequency method at high SNR.

VII. CONCLUSIONS

We find that the phase versus frequency fit and the Lorentzian nonlinear least squares fit are the most reliable procedures for estimating f_o and Q from complex transmission data. The Lorentzian fit of $|S_{21}|$ vs. frequency is surprisingly precise, but suffers from poor accuracy relative to vector methods, except for very noisy data. However, a major advantage of vector data is that it allows one to perform corrections to remove cross talk, delay, and nearby resonances, thus significantly improving the quality of subsequent fits. For the fixed-power measured data sets, the phase vs. frequency fit has the highest precision and accuracy in the determination of f_o and Q making it the best method overall. All of these methods are good for SNR greater than about 10. Below this value, all methods of determining Q and resonant frequency from complex transmission coefficient data degrade dramatically. Concerning robustness, the phase vs. frequency fit does well for a dynamic range of Q , while the Lorentzian fit does well in the power-ramp (SNR = 1 to 2000).

We also find that significant improvements can be made to the determination of resonant frequency and Q in noisy situations when careful attention is paid to the circle fitting procedure of the complex S_{21} data. Further development of the inverse mapping and Snortland methods can greatly improve the accuracy and precision of resonant frequency and Q determination in realistic measurement situations.

ACKNOWLEDGMENTS

We thank A. Schwartz and B. J. Feenstra for their critical reading of the manuscript, and H. J. Snortland and R. C. Taber for many enlightening discussions. This work is supported by the National Science Foundation through grant number DMR-9624021, and the Maryland Center for Superconductivity Research.

TABLES

TABLE I. Measurements of relative precision of the seven methods used to determine f_o and Q from complex transmission data. Tabulated are ratios of the standard deviation to the average values for both resonant frequency ($\sigma(f_o)/\overline{f_o}$) and quality factor ($\sigma(Q)/\overline{Q}$) normalized to the best value (given in parentheses), for SNR $\approx 49, 368$, and ramped from 5 to 168. All entries are based on measured data.

Precision Table	Noisy (P = +3 dBm, SNR ≈ 49)		Less Noisy (P = +15 dBm, SNR ≈ 368)		Power Ramp (SNR ≈ 5 to 168)	
Method	Q	f_o	Q	f_o	Q	f_o
3 dB	5.91	1.069	7.50	4.77	190.44	1.274
Lorentzian	1.55	1.025	2.27	1.10	1 (1.91 x 10 ⁻²)	1.004
RCA	5.66	1.030	5.24	1	11.04	1.031
Inverse Mapping	6.02	1.021	7.95	1.57	4.27	1.321
Modified Mapping	1.49	1.031	5.89	2.13	1.61	1 (7.17 x 10 ⁻⁹)
Phase vs. Freq	1 (2.51 x 10 ⁻³)	1 (1.15 x 10 ⁻⁸)	1 (2.80 x 10 ⁻⁴)	1 (3.12 x 10 ⁻¹⁰)	1.47	1.025
Snortland	2.27	1.029	2.09	1	5.98	1.086

TABLE II. Measurements of the relative accuracy of the seven methods used to determine f_o and Q from complex transmission data. Tabulated are ratios of the difference of the averages of f_o and Q from the known value divided by the known values, for both resonant frequency ($\frac{|\overline{f_o} - f_o^{known}|}{f_o^{known}}$) and quality factor ($\frac{|\overline{Q} - Q^{known}|}{Q^{known}}$). The entries are normalized to the best value (given in parentheses), for $Q = 10^3$, $Q = 10^5$ (both with $\text{SNR} \approx 65$), and SNR ramped from 1 to 2000. All entries are based on generated data.

Accuracy Table	$Q = 10^3$		$Q = 10^5$		Power Ramp (SNR \approx 1 to 2000)	
	Q	f_o	Q	f_o	Q	f_o
3 dB	253.08	217.39	240.21	117.15	401.48	43.87
Lorentzian	15.38	27.25	14.93	17.28	1 (3.11 x 10 ⁻²)	1 (1.46 x 10 ⁻⁹)
RCA	246.15	403.05	23.35	217.76	8.39	73.39
Inverse Mapping	3.85	3.01	10.43	2.21	2.84	5.72
Modified Mapping	2.77	3.5	5.64	1.57	1.83	8.43
Phase vs. Freq	1 (1.30 x 10 ⁻⁴)	1 (7.88 x 10 ⁻⁸)	1 (1.40 x 10 ⁻⁴)	1 (1.46 x 10 ⁻⁹)	4.03	12.00
Snortland	103.08	12.68	95.21	8.50	5.11	13.50

REFERENCES

- ¹ C. G. Montgomery, *Technique of Microwave Measurements*, MIT Rad. Lab. Series, Vol. 11 (McGraw-Hill, Inc. 1947).
- ² L. Malter, and G. R. Brewer, *J. Appl. Phys.*, **20**, 918 (1949).
- ³ E. L. Ginzton, *Microwave Measurements*, (McGraw-Hill Inc. 1957).
- ⁴ M. Sucher, and J. Fox, *Handbook of Microwave Measurements*, Vol. II, 3rd ed. (John Wiley & Sons, Inc. 1963), Chap. 8.
- ⁵ D. Kajfez, and E. J. Hwan, *IEEE Trans. Microwave Theory Tech.*, **MTT-32**, 666 (1984).
- ⁶ E. Sun, and S. Chao, *IEEE Trans. Microwave Theory Tech.* **43**, 1983 (1995).
- ⁷ M. B. Barmatz, *NASA Tech Brief*, **19**, No. 12, Item #16, (Dec. 1995).
- ⁸ H. Padamsee, J. Knobloch, and T. Hays, *RF Superconductivity for Accelerators*, (John Wiley & Sons, Inc. 1998).
- ⁹ A. F. Harvey, *Microwave Engineering*, (Academic Press 1963).
- ¹⁰ S. R. Stein, and J. P. Turneaure, *Electronics Letters*, **8**, 321 (1972).
- ¹¹ O. Klein, S. Donovan, M. Dressel, and G. Grüner, *International Journal of Infrared and Millimeter Waves*, **14**, 2423 (1993); S. Donovan, O. Klein, M. Dressel, K. Holczer, and G. Grüner, *International Journal of Infrared and Millimeter Waves*, **14**, 2459 (1993); M. Dressel, O. Klein, S. Donovan, and G. Grüner, *International Journal of Infrared and Millimeter Waves*, **14**, 2489 (1993)
- ¹² A. N. Luiten, A. G. Mann, and D. G. Blair, *Meas. Sci. Technol.*, **7**, 949 (1996).
- ¹³ J. E. Aitken, *Proc. IEE*, **123**, 855 (1976).
- ¹⁴ J. R. Ashley, and F. M. Palka, *The Microwave Journal*, 35 (June 1971).
- ¹⁵ K. Watanabe, and I. Takao, *Rev. Sci. Instrum.*, **44**, 1625 (1973).

- ¹⁶ V. Subramanian, and J. Sobhanadri, Rev. Sci. Instrum., **65**, 453 (1994).
- ¹⁷ M. C. Sanchez, E. Martin, J. M. Zamarro, IEE Proceedings, **136**, 147 (1989).
- ¹⁸ E. K. Moser, and K. Naishadham, IEEE Trans. on Appl. Superconductivity, **7**, 2018 (1997).
- ¹⁹ Z. Ma, Ph. D. Thesis, (Ginzton Labs Report No. 5298), Stanford University, (1995).
- ²⁰ K. Leong, J. Mazierska, and J. Krupka, 1997 IEEE MTT-S Proceedings.
- ²¹ H. J. Snortland, Ph. D. Thesis, (Ginzton Labs Report No. 5552), Stanford University, (1997). See also <http://loki.stanford.edu/Vger.html>. We used V'Ger version 2.37 for the analysis performed in this paper.
- ²² J. Mao, Ph. D. Thesis, University of Maryland, (1995).
- ²³ S. Sridhar, and W. L. Kennedy, Rev. Sci. Instrum., **59**, 531 (1988).
- ²⁴ W. H. Press, B. P. Flannery, S. A. Teukolsky, W. T. Vetterling, *Numerical Recipes*, (Cambridge University Press 1989), pp. 105, 202-203, 523-528.
- ²⁵ P. R. Bevington, *Data Reduction and Error Analysis for the Physical Sciences*, (McGraw-Hill, Inc. 1969), pp. 237-240.
- ²⁶ T. Miura, T. Takahashi, and M. Kobayashi, IEICE Trans. Electron., **E77-C**, 900 (1994).
- ²⁷ F. Gao, M. V. Klein, J. Kruse, and M. Feng, IEEE Trans. Microwave Theory Tech., **44**, 944 (1996).
- ²⁸ R. C. Taber, Hewlett-Packard Laboratories, private communication.
- ²⁹ R. V. Churchill, and J. W. Brown, *Complex Variables and Applications*, 5th Ed. (McGraw-Hill, Inc., New York) p. 209.
- ³⁰ The mapping defined by Eq. (15) maps lines of slope m through the pole in the frequency plane to lines of slope $-m$ through the origin in the S_{21} plane. Note the mapping defined

by Eq (15) is not conformal at the pole because it is not analytic there, however it is an isogonal mapping at that point. See reference 29.

³¹ M. H. Richardson and D. L. Formenti, Proc. International Modal Analysis Conference, 167 (1982).

³² The factor of 2 in front of the \tan^{-1} comes from the difference in angle subtended as seen from the origin vs. the center of the circle for a circle in canonical position in the S_{21} plane (Fig. 3 (b)).

FIGURES

FIG. 1. Measured magnitude of the complex transmission coefficient S_{21} of a superconducting resonator as a function of frequency for measured data (Input power = +10 dBm, SNR \approx 108). A Lorentzian curve is fit to the data as described in the text. Inset is the lumped element model circuit diagram for the resonator. The input and output transmission lines have impedance Z_o , l_{m1} and l_{m2} are coupling mutual inductances, C is the capacitance, R is the resistance, and L is the inductance of the model resonator.

FIG. 2. Measured imaginary vs. real part of the complex transmission coefficient S_{21} for a single resonant mode (Input power = +3 dBm, SNR \approx 49). This plot shows data and a circle fit, as well as the translated and rotated circle in canonical position. ($X \approx (1.67 \times 10^{-4}, -2.52 \times 10^{-4})$, $\phi \approx 116^\circ$). Large dots indicate centers of circles, and the size of the translation vector has been exaggerated for clarity.

FIG. 3. (a). The complex frequency plane is shown with frequency points f_1 , f_2 , and f_3 on the imaginary axis and a pole off of the axis. The imaginary frequency axis is mapped onto the complex S_{21} plane (b) as a circle in canonical position, and the corresponding frequency points are indicated on the circumference of the circle.

FIG. 4. Measured phase as a function of frequency for measured data (SNR \approx 31), both data and fit are shown. Inset is the translated and rotated circle, where its center is at the origin and the phase to each point is calculated from the positive real axis.

FIG. 5. Plot of fit resonant frequency versus trace number for measured data when the source power is +10 dBm. Results are shown for three methods discussed in the text.

FIG. 6. Plot of fit quality factor versus trace number for measured data when the power is +10 dBm. Results are shown for three methods discussed in the text.

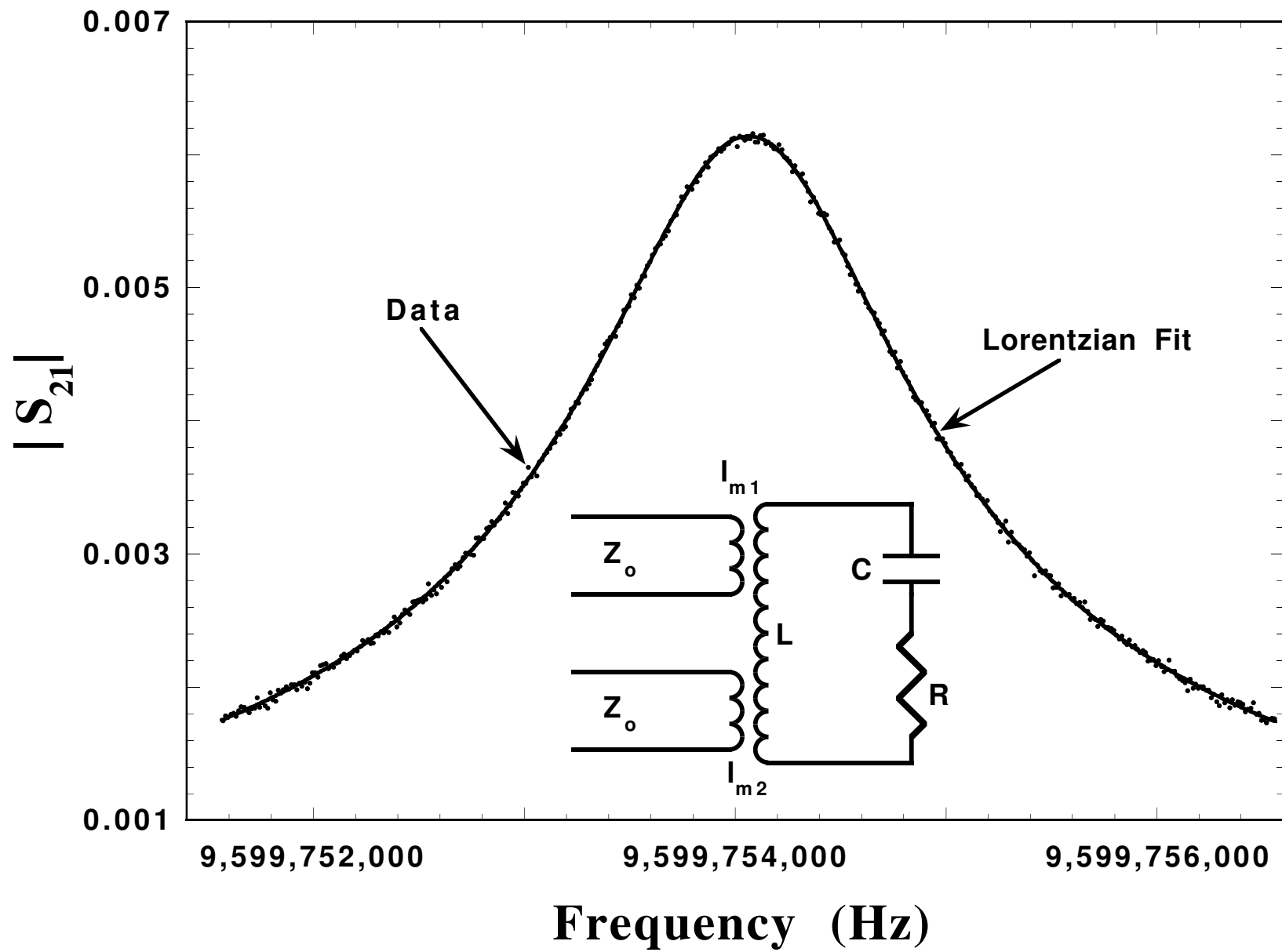
FIG. 7. Plot of fit resonant frequency versus the signal-to-noise ratio on a log scale for the measured power-ramped data set. Results are shown for three methods discussed in the text.

FIG. 8. Plot of fit quality factor versus the signal-to-noise ratio on a log scale for the measured power-ramped data set. Results are shown for three methods discussed in the text.

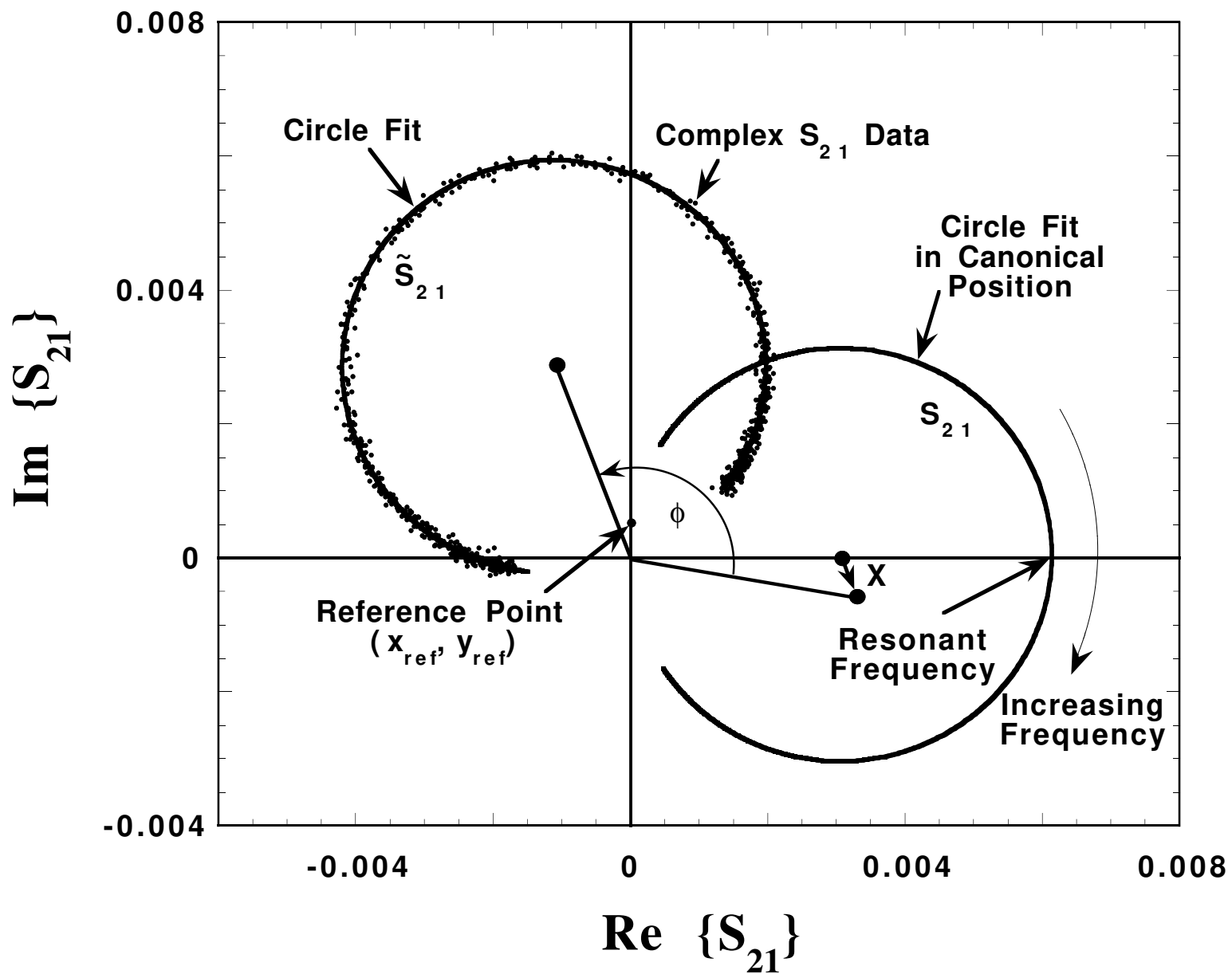
FIG. 9. Measured imaginary vs. real part of the complex transmission coefficient for measured data (SNR ≈ 4 , $X \approx (7.22 \times 10^{-5}, 3.26 \times 10^{-4})$, $\phi \approx 220^\circ$). Plot shows data and two circle fits, one where the standard weighting is used (dashed line), and one where the square root radial weighting is used (solid line).

FIG. 10. The calculated circle fit radius vs. the signal-to-noise ratio on a log scale is shown for the generated power-ramped data set. The plot shows the results from four different weightings: W_{Std} , W_{Radial} , W_{Radial}^2 , $W_{Radial}^{1/2}$. The true value for the radius is 0.2.

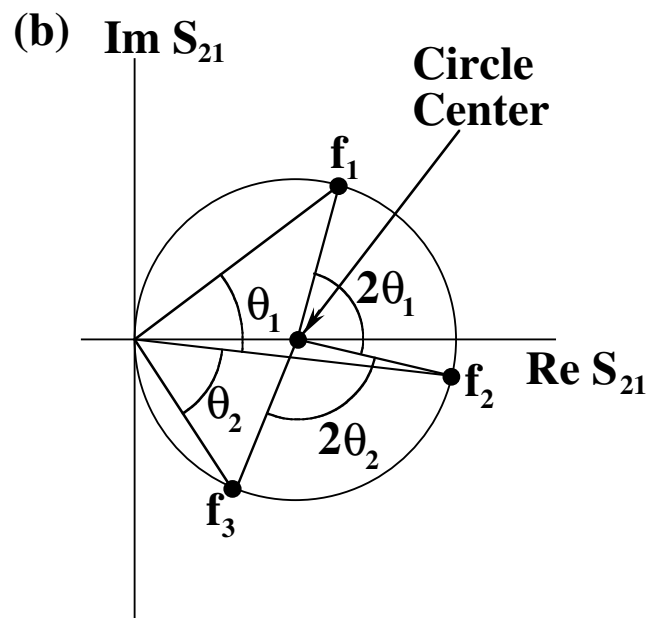
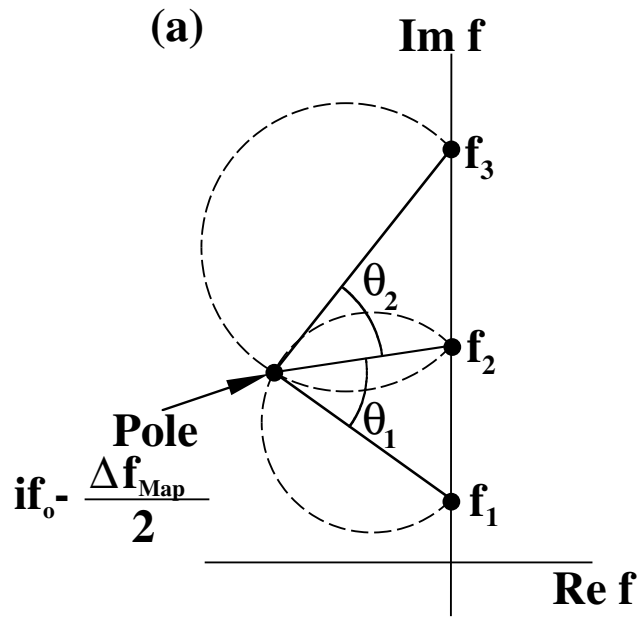
FIG. 11. The normalized error in the determination of the center of the fit circle is shown vs. the signal-to-noise ratio on a log scale for the generated power-ramp data. Results are from the weightings: W_{Std} , W_{Radial} , W_{Radial}^2 , $W_{Radial}^{1/2}$. Inset (a) is a plot of the true circle (solid line) and the fit circle to the data (dashed line) to show that the determination of the center from the fit (x_{fit}, y_{fit}) is located at an angle α from the line connecting the true center (x_c, y_c) to the resonant frequency point, f_o . The distance from the true center to the calculated center is related to the normalized error in the calculated center E_c . Inset (b) is a plot of the angle α vs. log of SNR for the generated data.



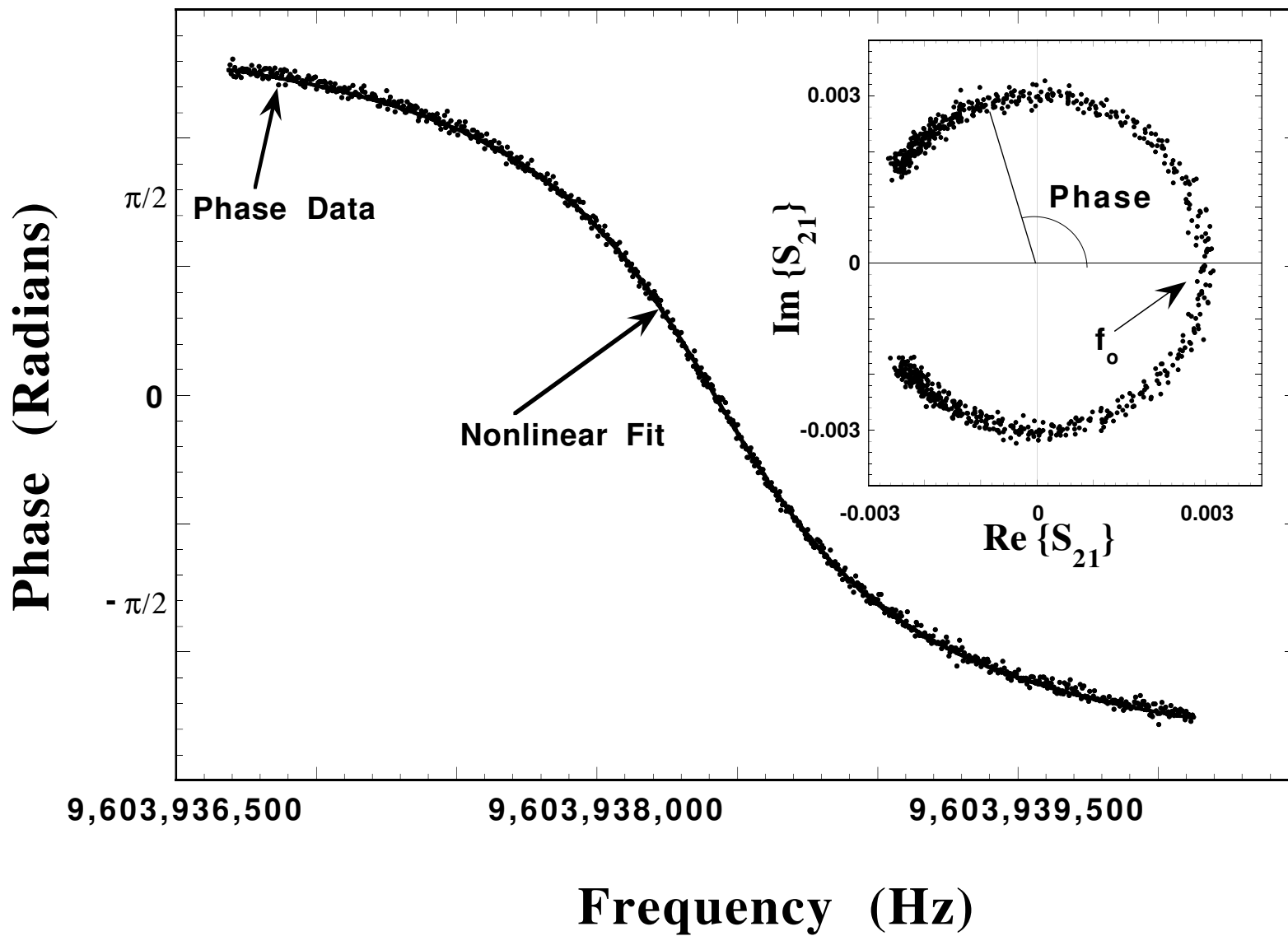
Petersan
Figure 1



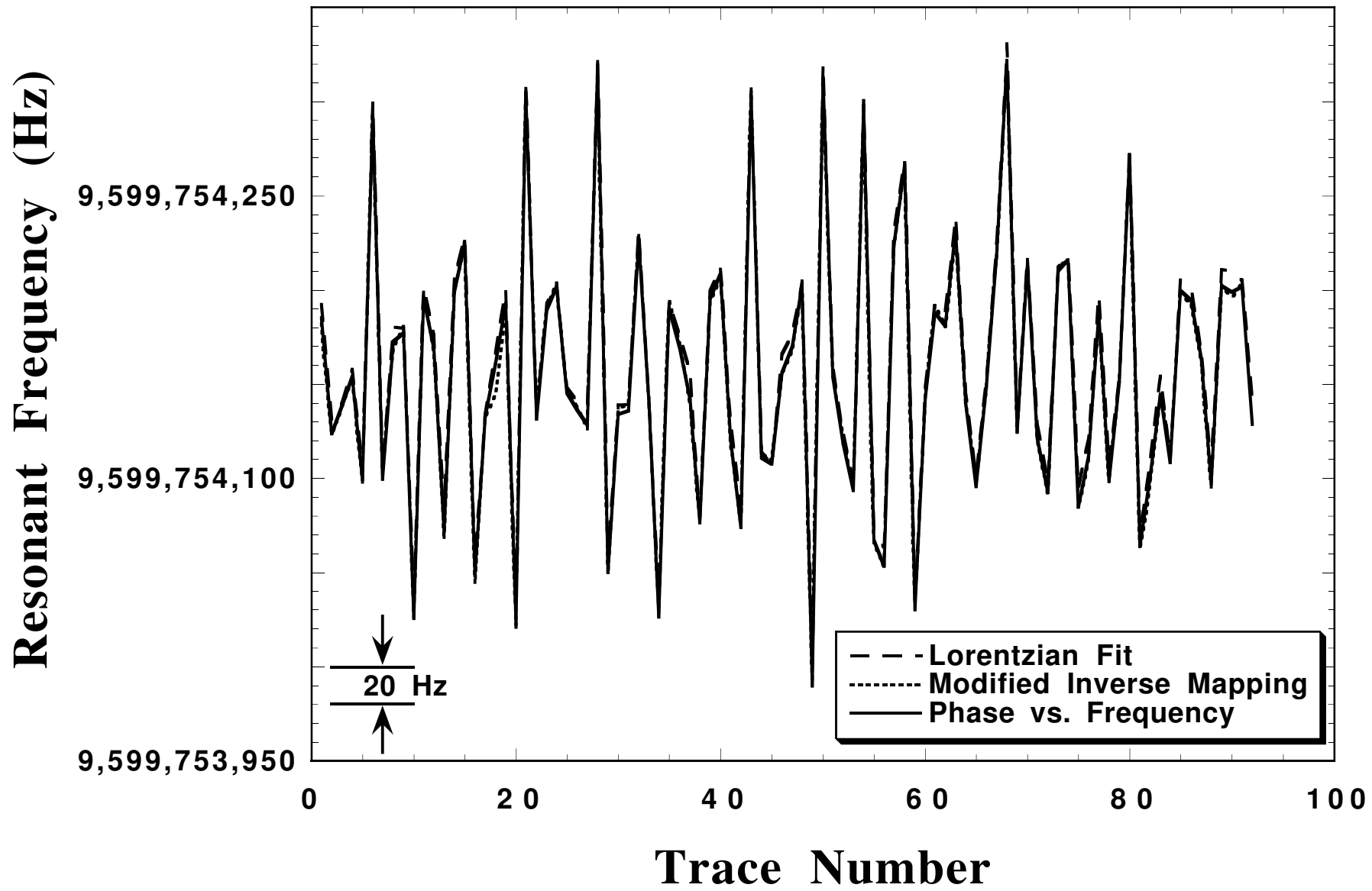
Petersan
 Figure 2



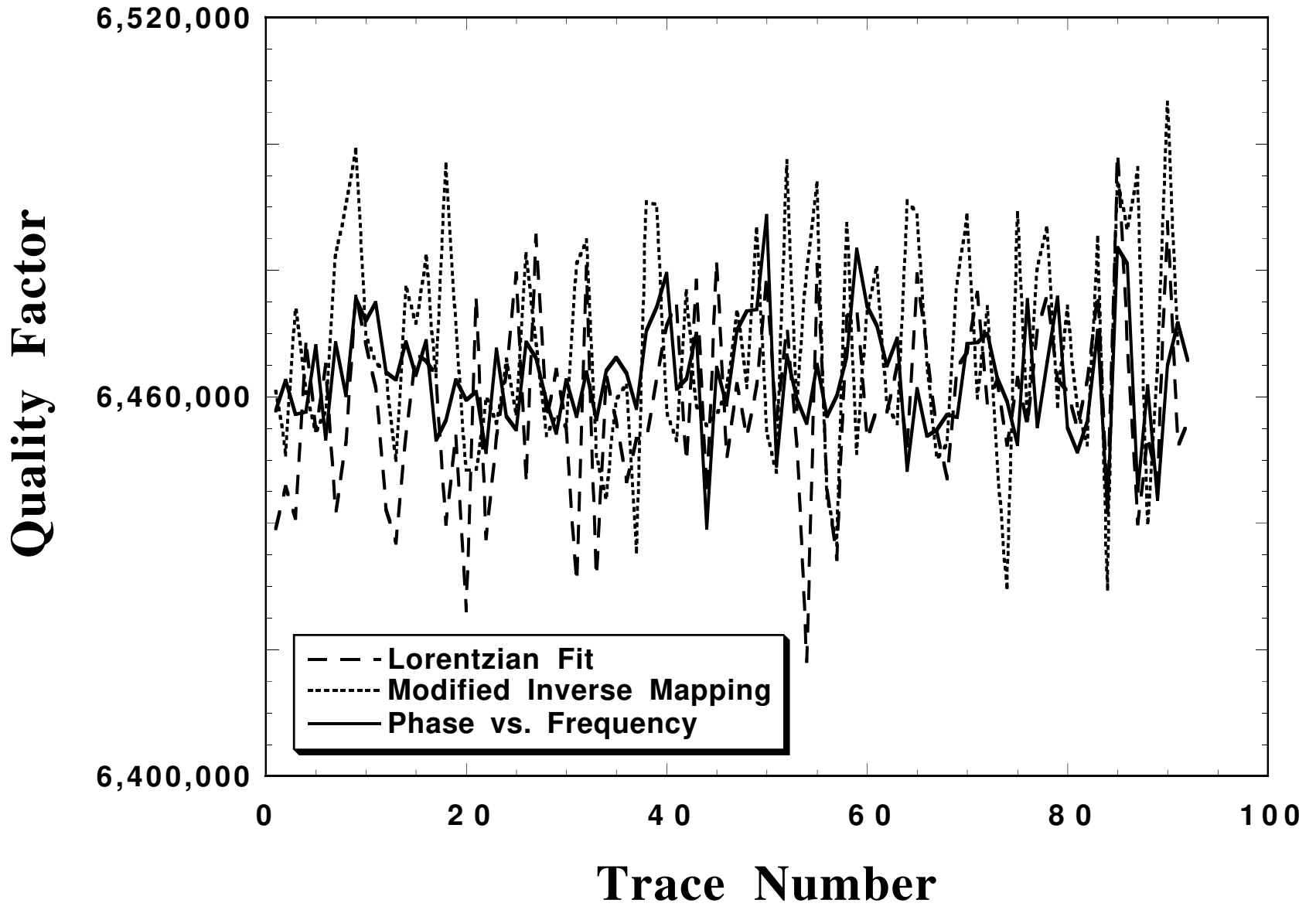
Petersan
Figure 3



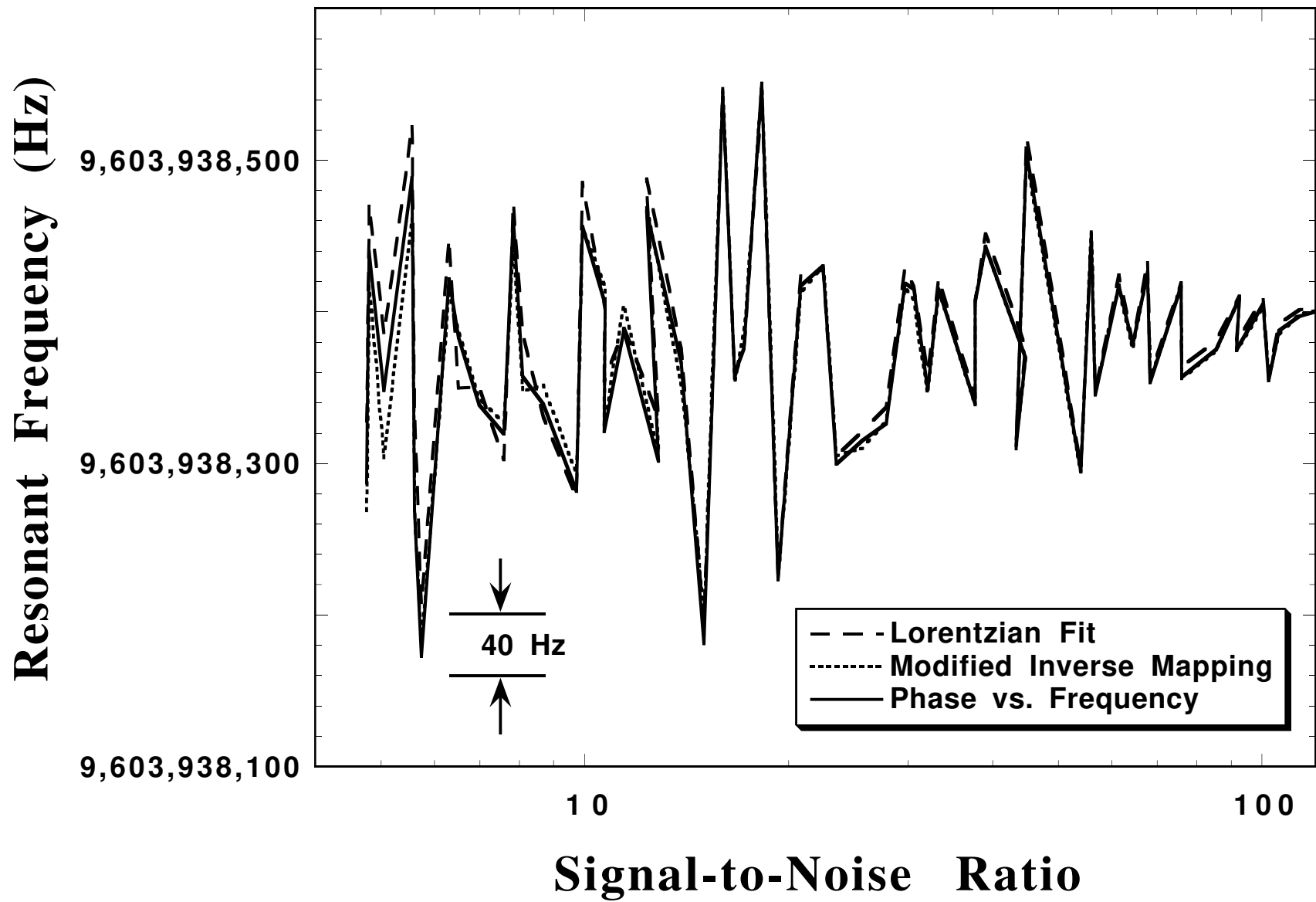
Petersan
Figure 4



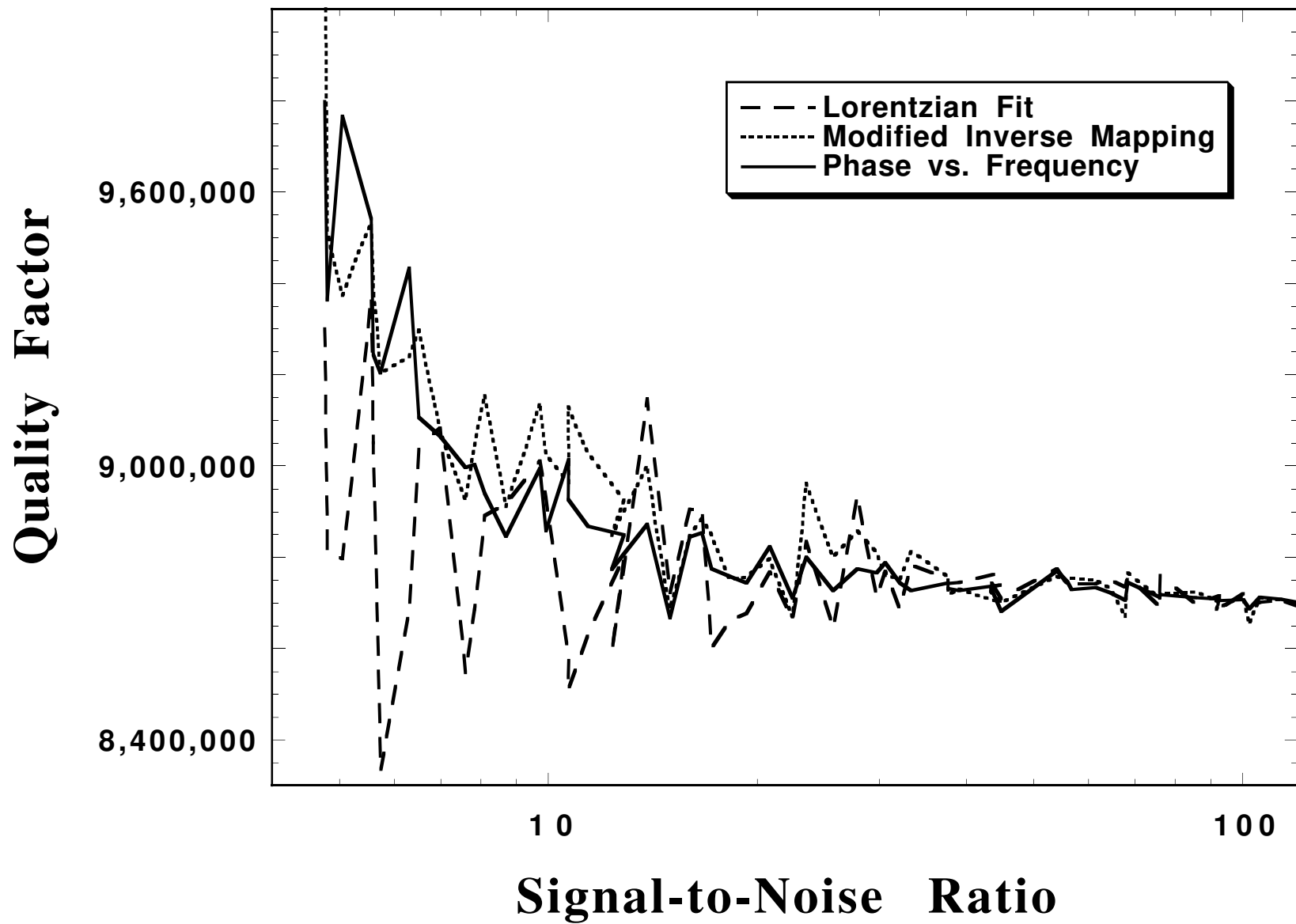
Petersan
Figure 5



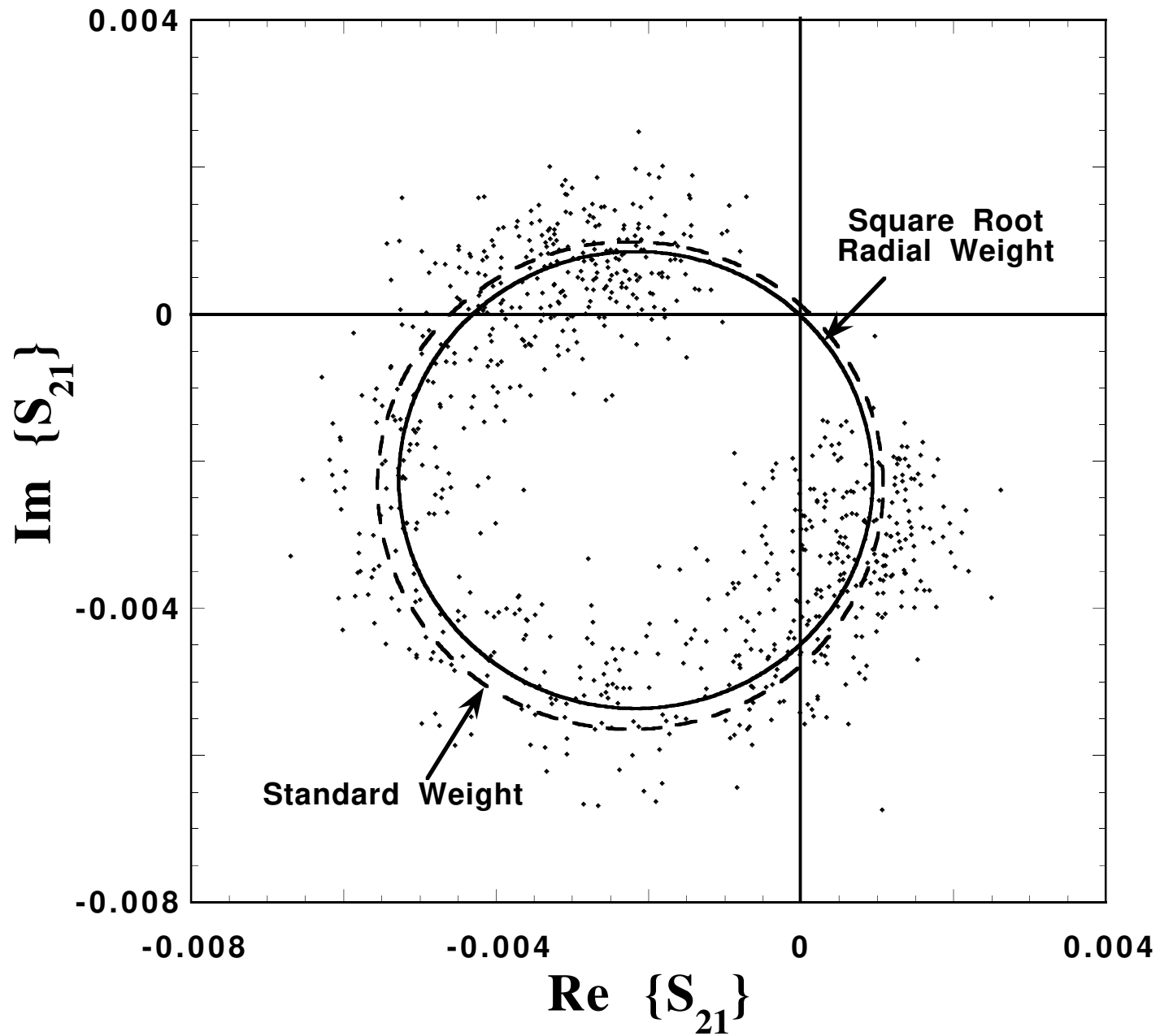
Petersan
Figure 6



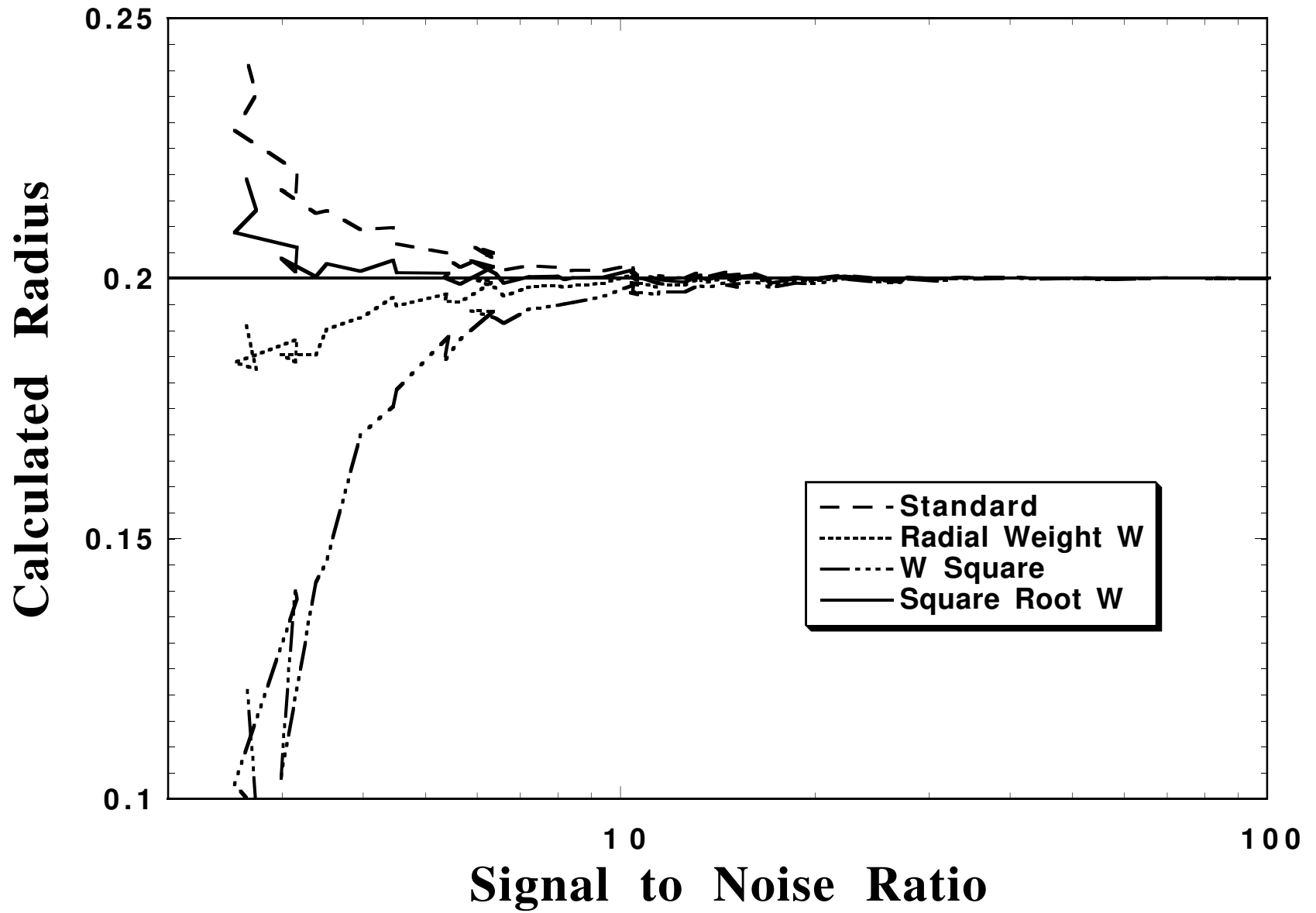
Petersan
Figure 7



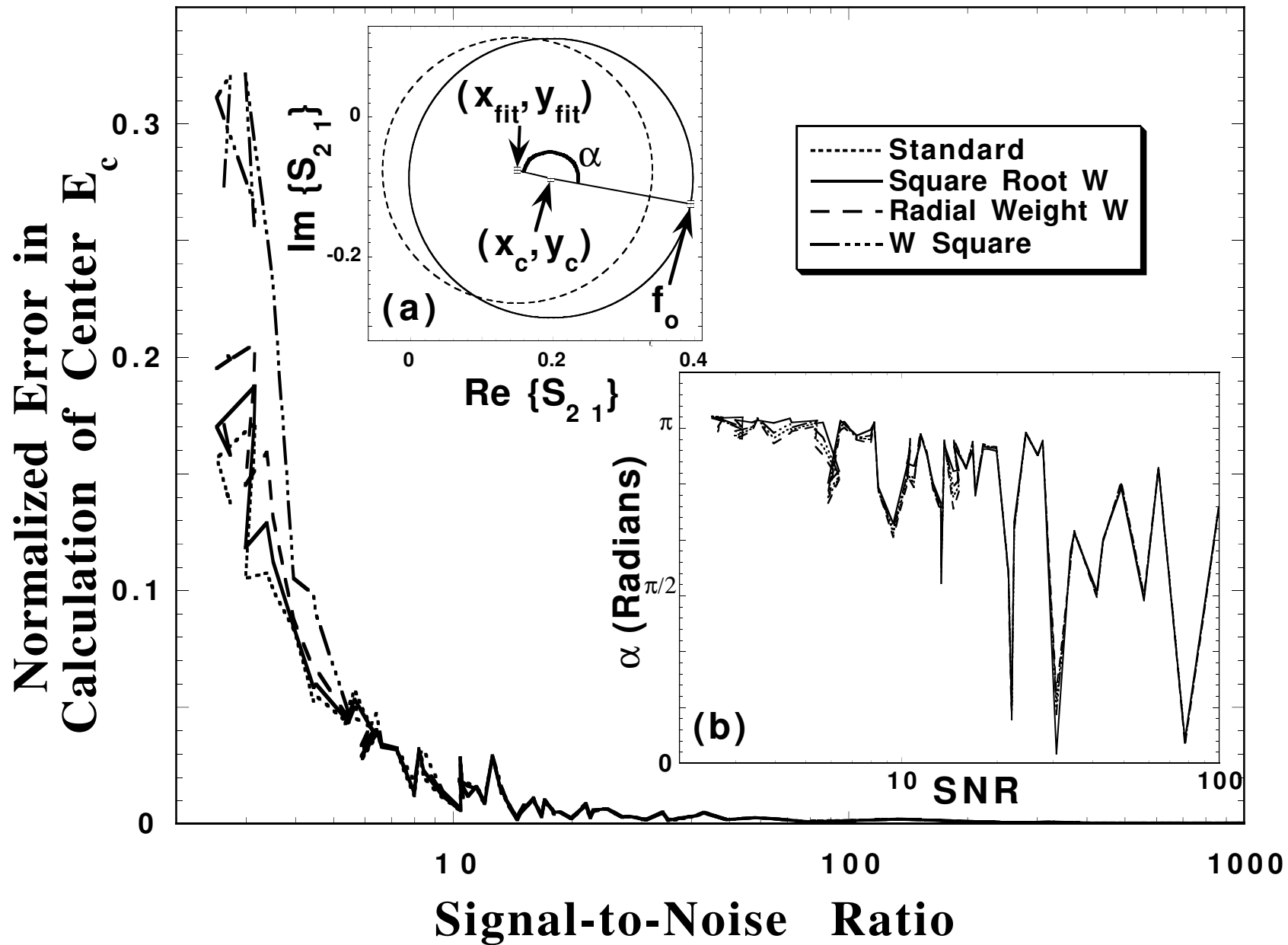
Petersan
Figure 8



Petersan
Figure 9



Petersan
Figure 10



Petersan
Figure 11